

RESEARCH

Open Access



Computational and pharmacokinetics studies of 1,3-dimethylbenzimidazolinone analogues of new proposed agent against Alzheimer's disease

Abduljelil Ajala^{*} , Adamu Uzairu, Gideon Adamu. Shallangwa and Stephen Eyije. Abechi

Abstract

Background: Alzheimer's disease (AD) is a multifactorial disorder that gradually destroys wisdom and memory skills. Currently, this disease can only be treated palliatively. However, the molecular mechanisms underlying this condition remain elusive. Therefore, these treatments are inadequate. Current medications can only increase patient warning signs. Chemical structures were drawn using Chemsketch software. Spartan'14 software was used to optimize the structures using density functional theory (DFT). The PaDEL software was used to generate the descriptors. The genetic function algorithm (GFA) and multi-linear regression (MLR) approaches were used to generate the QSAR model.

Results: In the present study, we performed a computational investigation, molecular docking, and pharmacokinetics analysis of 1,3-dimethylbenzimidazolinone derivatives. The descriptors generated in the model are AATS7i, MAT55p, SpMin7_Bhe, and GATS6c. Compounds 13 and 21 have the best binding scores, 11.2 kcal/mol and 10.8 kcal/mol, respectively, and optimal protein–ligand interactions with AChE. These compounds have brilliant pharmacokinetic and physicochemical properties.

Conclusions: The model was validated and found to have good internal and external assessment parameters: $R^2 = 0.937$, $R_{adj}^2 = 0.863$, $Q_{cv}^2 = 0.788$, $R_{test}^2 = 0.756$, $LOF = 0.0268$, $cR_p^2 = 0.677$. In summary, these data suggested that compounds 13 and 21 are promising multifunctional agents against AD.

Keywords: Alzheimer's disease, Docking, Pharmacokinetics, CADD, Validation, Descriptor

1 Background

Alzheimer's disease (AD) affects modern societies. AD is a product of dementia and a serious health problem worldwide. Today, the number of people living with dementia is estimated at 50.0 million worldwide, and by 2040, it may increase to 130.0 million, which is responsible for approximately 73% of the cases [1]. In the light of these realities, we may expect over 90 million AD

patients in the next three to four decades [1]. Deposits [2, 3], oxidative stress [3, 4], and low levels of acetylcholine [4–6] have all been proposed as sources of AD, and several drugs have been introduced into the market for the treatment of AD, especially those approved by the US government. They are six in number. Neuronal death cannot be slowed or stopped by any drug. The signs of AD have been improved by the introduction of drugs [7]. A few drugs include donepezil, galantamine, rivastigmine, and memantine [8].

AD remains irredeemable owing to the limited availability and low efficacy of drugs. Many researchers

*Correspondence: abdulajala39@gmail.com
Department of Chemistry, Faculty of Physical Sciences, Ahmadu Bello University, P.M.B. 1044, Zaria, Kaduna State, Nigeria

worldwide have intensified their efforts to find effective novel drugs and new biological targets.

To improve the drug improvement process in a more cost-efficient manner and to reduce failures in the final stage, the engagement of CADD techniques became indispensable for the initial stage of the drug discovery process. Valued evidence about the interface pattern between the protein and ligand, as well as the binding affinity, is a parameter for rational drug design, which provides a knowledge-driven method that will provide maximum output. In this study, a structure-based modelling approach was employed, using the 3D structure of the protein target for the screening of potential modulators, followed by biologically tested synthesized compounds and optimization. The best model was selected among the generated models based on statistical validity and was used for structural optimization to enhance potency and identify new chemical compounds in the in silico virtual screening of a large chemical catalogue [9, 10]. The rationale behind the work is $Y = A_1x_1 + A_2x_2 + A_3x_3 + B$. Y is the activity (pIC_{50}), where “ A ”s and “ x ”s are regression coefficients for conforming nonpartisan variables that represent molecular descriptors of molecules; “ A ”s correspond to “ X ”s. the last variable, “ B ”, is the regression constant.

The present study aimed to use QSAR, molecular docking simulation, in silico design, and ADMET properties to identify new drugs that are efficient against AD.

2 Methods

2.1 Data set gathering and activities

The data were obtained from the literature [11] as potential compounds against Alzheimer’s disease. Twenty-six derivatives of the compounds were extracted and selected for modelling. A list of the compounds is presented in Table 1. Data are presented as IC_{50} values (μM). The concentration was converted to the pIC_{50} by taking the inverse logarithm of each value. The residual value is the difference between the observed and calculated values, as listed in Table 1. The test set is represented by an * sign.

2.2 Molecular optimization and generation of molecular properties

All inhibitory compounds were optimized using the 1.1.4 version of Spartan software to attain a steady conformation at minimum energy. Lateral optimization processes were achieved with the help of the mechanical force field and density functional theory (DFT) [12]. V.2.2.0 of PaDEL software was used to generate 1800 descriptors, which simply describe the relationship between the experimental activity and the molecular structure of each molecule.

2.3 Data normalization, pretreatment, and training and test set generation

Each variable influences a good model to generate a good model. Therefore, the descriptor values generated from PaDEL software V2.20 were normalized using Eq. (1) to give the descriptor an equal chance at the inception [13, 14].

$$A = \frac{X_i - X_{\min}}{X_{\max} - X_{\min}} \quad (1)$$

where X_{\max} and X_{\min} are the maximum and minimum values of each descriptor, respectively. X_i is the value for each descriptor molecule. Afterwards, the normalized data were pretreated with pretreatment software (<https://dtclab.webs.com/software-tools>) to eliminate redundant molecular properties. The dataset was divided into a ratio of 7:3 that is the training and test sets, using the algorithm of Kennard and Stone, which was incorporated into the DTC lab software. Model and internal validation tests were confirmed using the training set. Meanwhile, the developed model was performed on a test set [15].

2.4 Derivation of the model and models and validation

Multi-variant equations (models) were generated using the multi-linear regression approach (MLR) and genetic function approximation (GFA), and Material Studio software V.8.0 was used to confirm the robustness and predictability of the built model.

2.5 Leverage applicability domain (LAD)

In vividly determining that a compound is an outlier, leverage values and standardized residuals are used together in what is called a Williams graph to describe the LAD of a given model. Influential and outlier molecules present in the dataset were determined using this approach, the leverage (hi) approach is defined in Eq. (2) and was used to define the domain space ± 2.5 for outlier molecules [15].

$$hi = Wi(W^T W)^{-1} W_i^T \quad (2)$$

where W_i represents the matrix of i in the training set. W represents the $n \times d$ matrix descriptor for the training set. W^T is the transpose of training set (W) represents the transposed matrix and W_i . The warning leverage k^* defined in Eq. (3) is the boundary for establishing the presence of an influential molecule.

$$k^* = 3 \frac{(x + 1)}{A} \quad (3)$$

Table 1 Molecular structures of inhibitory compound

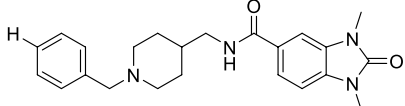
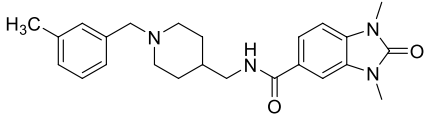
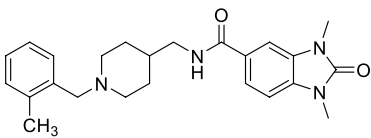
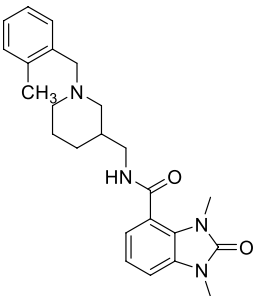
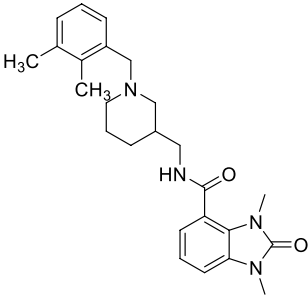
S/N	Molecular structures	Experimental activity PIC ₅₀	Calculated activity	Residual
1	 <i>N</i> -((1-benzylpiperidin-4-yl)methyl)-1,3-dimethyl-2-oxo-2,3-dihydro-1 <i>H</i> -benzo[d]imidazole-5-carboxamide	0.9074	0.7266	0.1808
2	 1,3-dimethyl- <i>N</i> -((1-(3-methylbenzyl)piperidin-4-yl)methyl)-2-oxo-2,3-dihydro-1 <i>H</i> -benzo[d]imidazole-5-carboxamide	0.5832	0.6218	0.0386
3	 1,3-dimethyl- <i>N</i> -((1-(2-methylbenzyl)piperidin-4-yl)methyl)-2-oxo-2,3-dihydro-1 <i>H</i> -benzo[d]imidazole-5-carboxamide	1.4101	1.3564	0.0537
4	 1,3-dimethyl- <i>N</i> -((1-(2-methylbenzyl)piperidin-3-yl)methyl)-2-oxo-2,3-dihydro-1 <i>H</i> -benzo[d]imidazole-4-carboxamide	0.9987	1.2220	0.2234
5	 <i>N</i> -((1-(2,3-dimethylbenzyl)piperidin-3-yl)methyl)-1,3-dimethyl-2-oxo-2,3-dihydro-1 <i>H</i> -benzo[d]imidazole-5-carboxamide	0.7135	0.7276	0.0141

Table 1 (continued)

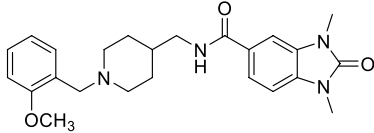
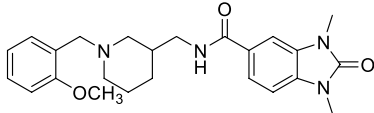
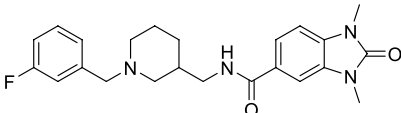
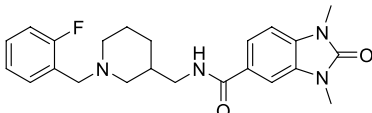
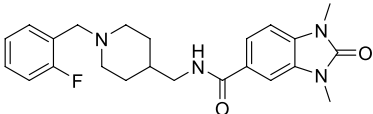
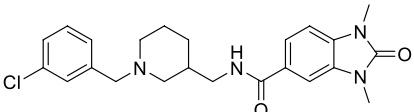
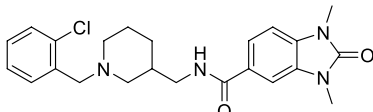
6				
	<i>N</i> -((1-(2-methoxybenzyl)piperidin-4-yl)methyl)-1,3-dimethyl-2-oxo-2,3-dihydro-1 <i>H</i> -benzo[d]imidazole-5-carboxamide	1.2092	1.1159	0.0933
7				
	<i>N</i> -((1-(2-methoxybenzyl)piperidin-3-yl)methyl)-1,3-dimethyl-2-oxo-2,3-dihydro-1 <i>H</i> -benzo[d]imidazole-5-carboxamide	0.4669	0.5519	0.0850
8				
	<i>N</i> -((1-(3-fluorobenzyl)piperidin-3-yl)methyl)-1,3-dimethyl-2-oxo-2,3-dihydro-1 <i>H</i> -benzo[d]imidazole-5-carboxamide	0.5932	0.7792	0.1859
9				
	<i>N</i> -((1-(2-fluorobenzyl)piperidin-3-yl)methyl)-1,3-dimethyl-2-oxo-2,3-dihydro-1 <i>H</i> -benzo[d]imidazole-5-carboxamide	0.7782	0.6662	0.1120
10*				
	<i>N</i> -((1-(2-fluorobenzyl)piperidin-4-yl)methyl)-1,3-dimethyl-2-oxo-2,3-dihydro-1 <i>H</i> -benzo[d]imidazole-5-carboxamide	0.6778	0.6853	0.0075
11				
	<i>N</i> -((1-(3-chlorobenzyl)piperidin-3-yl)methyl)-1,3-dimethyl-2-oxo-2,3-dihydro-1 <i>H</i> -benzo[d]imidazole-5-carboxamide	0.9479	0.9215	0.0265
12				
	<i>N</i> -((1-(2-chlorobenzyl)piperidin-3-yl)methyl)-1,3-dimethyl-2-oxo-2,3-dihydro-1 <i>H</i> -benzo[d]imidazole-5-carboxamide	1.5807	1.4568	0.1239

Table 1 (continued)

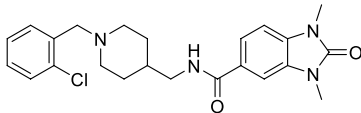
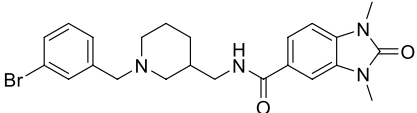
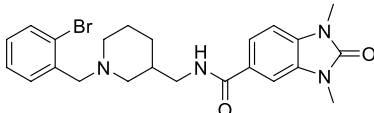
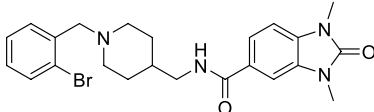
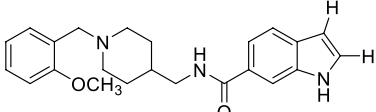
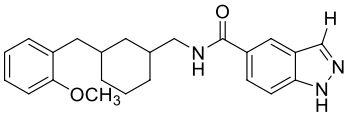
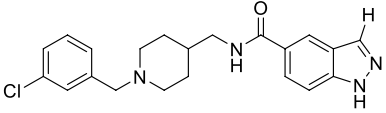
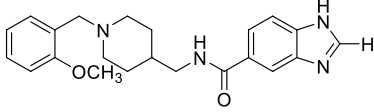
13		-		
	<i>N</i> -((1-(2-chlorobenzyl)piperidin-4-yl)methyl)-1,3-dimethyl-2-oxo-2,3-dihydro-1 <i>H</i> -benzo[d]imidazole-5-carboxamide	0.7356	0.8663	0.1307
14				
	<i>N</i> -((1-(3-bromobenzyl)piperidin-3-yl)methyl)-1,3-dimethyl-2-oxo-2,3-dihydro-1 <i>H</i> -benzo[d]imidazole-5-carboxamide	0.8739	0.7697	0.1042
15*				
	<i>N</i> -((1-(2-bromobenzyl)piperidin-3-yl)methyl)-1,3-dimethyl-2-oxo-2,3-dihydro-1 <i>H</i> -benzo[d]imidazole-5-carboxamide	0.3372	0.3181	0.0192
16*				
	<i>N</i> -((1-(2-bromobenzyl)piperidin-4-yl)methyl)-1,3-dimethyl-2-oxo-2,3-dihydro-1 <i>H</i> -benzo[d]imidazole-5-carboxamide	0.9708	0.9647	0.0061
17				
	<i>N</i> -((1-(2-methoxybenzyl)piperidin-4-yl)methyl)-1 <i>H</i> -indole-6-carboxamide	0.0170	0.1953	0.1783
18				
	<i>N</i> -((3-(2-methoxybenzyl)cyclohexyl)methyl)-1 <i>H</i> -indazole-5-carboxamide	0.8239	0.9172	0.0933
19				
	<i>N</i> -((1-(3-chlorobenzyl)piperidin-4-yl)methyl)-1 <i>H</i> -indazole-5-carboxamide	0.2900	0.1465	0.1436
20				
	<i>N</i> -((1-(2-methoxybenzyl)piperidin-4-yl)methyl)-1 <i>H</i> -benzo[d]imidazole-5-carboxamide	0.3768	0.3735	0.0033

Table 1 (continued)

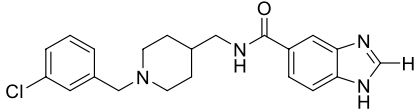
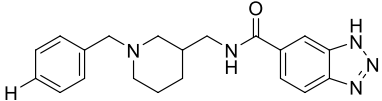
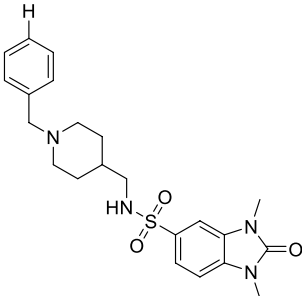
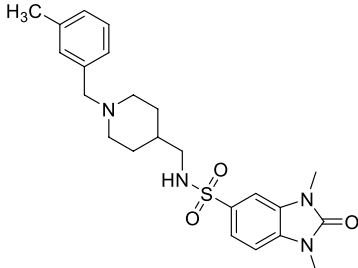
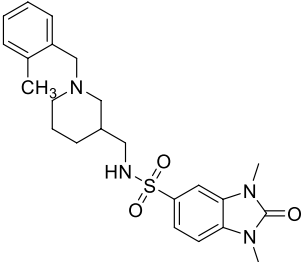
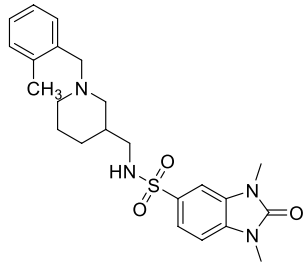
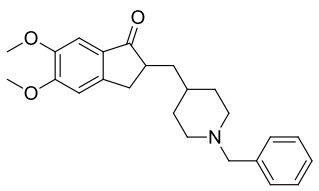
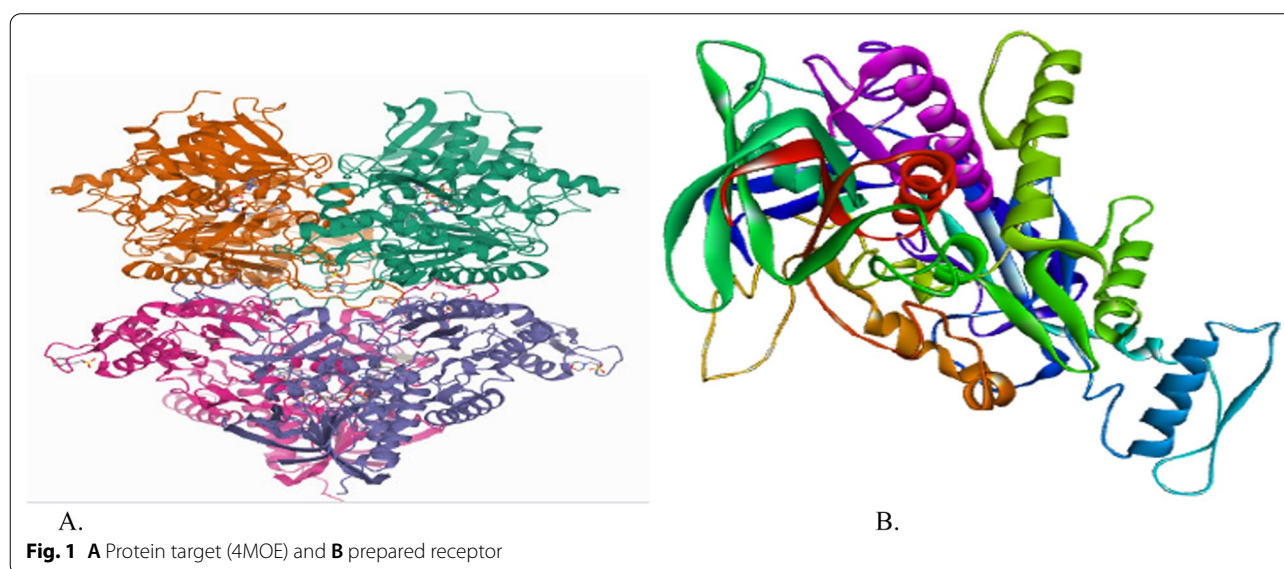
21				
	<i>N</i> -((1-(3-chlorobenzyl)piperidin-4-yl)methyl)-1 <i>H</i> -benzo[<i>d</i>]imidazole-5-carboxamide	0.6721	0.4607	0.2114
22				
	<i>N</i> -((1-benzylpiperidin-3-yl)methyl)-1 <i>H</i> -benzo[<i>d</i>][1,2,3]triazole-6-carboxamide	0.5670	0.4645	0.1025
23				
	<i>N</i> -((1-benzylpiperidin-4-yl)methyl)-1,3-dimethyl-2-oxo-2,3-dihydro-1 <i>H</i> -benzo[<i>d</i>]imidazole-5-sulfonamide	1.0438	0.4949	0.5489
24*				
	1,3-dimethyl- <i>N</i> -((1-(3-methylbenzyl)piperidin-4-yl)methyl)-2-oxo-2,3-dihydro-1 <i>H</i> -benzo[<i>d</i>]imidazole-5-sulfonamide	0.4089	0.3314	0.0775
25*				
	1,3-dimethyl- <i>N</i> -((1-(2-methylbenzyl)piperidin-3-yl)methyl)-2-oxo-2,3-dihydro-1 <i>H</i> -benzo[<i>d</i>]imidazole-5-sulfonamide	0.2676	0.3321	0.0645

Table 1 (continued)

26*	1,3-dimethyl- <i>N</i> -((1-(2-methylbenzyl)piperidin-3-yl)methyl)-2-oxo-2,3-dihydro-1 <i>H</i> -benzo[<i>d</i>]imidazole-5-sulfonamide		1.3939	0.3204	1.0735
27		Donepezil	0.4089	0.2756	0.1333



where A and x are the total number of training set and descriptors present in the built model.

2.6 Y-randomization validation and Confirmation of the build model

To investigate the robustness of the developed models and determine whether the models were the result of chance correlations [16, 17],

A Y-randomization test was applied to the final model. Here, the activity value is randomly permuted and a new QSAR model will be constructed using the optimum

descriptors in the final models as reported in the literature [18]. This new model is expected to report R^2 and Q^2 values that are very low for several trials compared to those reported by the original models. For clarity, this procedure was repeated 100 times. The conditions for authenticating both the test and the training set were stated and related to the commonly accepted threshold value shown in Table 6 for any QSAR model [19, 20] to assert the consistency, fitting, stability, strength, and predictability of the developed models.

Table 2 Descriptors used in the model

Descriptor	Type	Significance	Class	Contribution
AATS7s	Autocorrelation	Average Moreau–Broto autocorrelation-lag 7/weighted by I-state autocorrelation descriptor	2D	Positive
MATS5p	Autocorrelation	Moran autocorrelation-lag 5/weighted by polarizabilities	2D	Positive
GATS6c	Autocorrelation	Geary autocorrelation-lag 6/weighted by charges	2D	Negative
SpMin7_Bhe	Autocorrelation	Burden modified eigenvalues descriptors	2D	Positive

2.7 Docking studies

2.7.1 Receptor and ligand preparation

The acetylcholinesterase receptor (4MOE) crystal with a low resolution shown in Fig. 1A was downloaded from the PDB (www.rcsb.org). Using the Visualizer software in Discovery Studio, completely imported foreign matter such as cofactors and ligands associated with the enzyme were removed, and the target protein was saved in the PDB format. Next, the target protein saved in PDB format was imported into PyRx software and converted into macromolecules (Fig. 1B). The Spartan software, an optimizing tool, was used to attain the unchanging minimal energy of the benzimidazolinone derivative conformation. The optimized ligands were saved in PDB format, recognized by PyRx software, and converted to micro molecules (pdbqt).

2.7.2 Docking of receptor and ligand

PyRx virtual screening software was used to perform ligand–receptor interactions and molecular docking of benzimidazolinone derivatives. AutoDock Vina and AutoDock 4.2 in PyRx software were used as the docking software. Discovery Studio Visualizer software, V 2016, was used to create and investigate the docked results [21].

2.8 Drug-likeness and prediction of ADMET

Hypothetically derived statistical models are generated by in silico approaches for the determination of absorption distribution, metabolism excretion, and toxicity (ADMET) parameters, which are produced by relating the structural features of compounds. They have been measured in a given assay to their biological response, and are now commonly used because of their low resource requirements [21]. Therefore, two out of twenty-six compounds that showed reasonable binding modes with AChE based on similar binding patterns to donepezil and advanced negative binding affinity, were subjected to physicochemical studies. Studies were carried out using the Swiss online ADMET web tool [22] to evaluate the model for physicochemical properties, pharmacokinetics, drug-likeness, and medicinal chemistry friendliness, including in-house proficient methods such as the BOILED-egg, ILOGP, and Bio-availability Radar of the selected compounds. A diagram of

WLOGP versus TPSA was plotted to determine the blood–brain barrier (BBB) and human gastrointestinal absorption ability of the compounds [22].

3 Results

3.1 QSAR analysis

The best model for predicting the derivatives of 1, 3-dimethylbenzimidazolinone against AD was successfully achieved by adopting the techniques of the computational method. A dataset of 26 molecules was split into 20 training sets and 6 test sets using the method of Ambure and his research group [23]. QSAR models were derived using the MLR technique from 20 training set compounds, which also served as a data set for internal validation tests and the validation of the model was conducted on the test set.

3.2 Constructed model

$$\text{PIC}_{50} = 11.585405732 \times \text{AATS7i} + 0.212053417 \times \text{MATS5p} + 0.230548471 \times \text{SpMin7_Bhe} - 0.753332018 \times \text{GATS6c} + 2.057162$$

Table 3 Statistical consideration to validate the descriptors

Descriptor	Xj	AM	P value	VIF	SE
Hmin	9.362702	4.61	0.002032	3.787947	2.5135
Apol	−0.01584	0.91	0.160129	2.466789	0.010718
MDEC-23	0.143867	0.09	0.000173	1.156238	0.029033
Weta3.polar	0.690708	2.59	0.118696	2.014014	0.417352

Table 4 Validation of the descriptors using Pearson's correlation matrix

	hmin	apol	MDEC-23	Weta3.polar
hmin	1			
apol	−0.70674	1		
MDEC-23	−0.03149	−0.22711	1	
Weta3.polar	−0.68057	0.349355	0.016518	1

Table 5 Validation parameters to confirm the built model

Validation bounds	Mathematical expression	Threshold	Model	Comment	Ref
Friedman LOF	$\frac{SEE}{\left(1 - \frac{c+d \times p}{N}\right)^2}$	Significantly low	0.0268	Passed	[24]
R^2	$1 - \frac{\sum (Y_{exp} - Y_{pred})^2}{\sum (Y_{exp} - Y_{train})^2}$	$R^2 > 0.6$	0.9062	Passed	[24]
R^2_{adj}	$\frac{R^2 - p(n-1)}{n-p-1}$	$R^2_{adj} > 0.6$	0.863	Passed	[24]
Q^2_{cv}	$1 - \frac{\sum (Y_{pred} - Y_{exp})^2}{\sum (Y_{exp} - Y_{train})^2}$	$Q^2_{cv} > 0.6$	0.788	Passed	[24]
Significant regression			Yes	Passed	
F-value (95%)	$\frac{\sum (Y_{pred} - Y_{exp})^2}{p} / \frac{\sum (Y_{pred} - Y_{exp})^2}{N-p-1}$	$F_{(test)} > 2.09$	3.001	Passed	[24]
Min exp error for non-significant			0.0739	Passed	[17]

Table 6 Y-randomization parameters test

Model	R	R^2	Q^2
Original	0.897695	0.805857	0.617385
Random 1	0.726183	0.527341	0.085324
Random 2	0.424387	0.180104	-0.64949
Random 3	0.456764	0.208633	-0.55097
Random 4	0.573928	0.329394	-0.08597
Random 5	0.685618	0.470072	0.001947
Random 6	0.324353	0.105205	-0.63431
Random 7	0.344707	0.118823	-0.70223
Random 8	0.36793	0.135372	-0.55566
Random 9	0.511569	0.261703	-0.46915
Random 10	0.448211	0.200893	-0.40465

The experimental activities reported in the literature and the theoretical activities calculated for all the anti-Alzheimer compounds are presented in Table 1. The residual value, which is the difference between the experimental and theoretical activities, was observed to be significantly low. A low residual value indicates predictability of the model. The best descriptors that efficiently described the anti-Alzheimer compounds in relation to their

experimental activities selected by the GFA approach are reported in Table 2.

3.3 Mechanistic information of descriptors in the model built

Table 2 provides a comprehensive description of the molecular descriptors in the constructed model.

3.4 Derivation of the model and models and validation

Table 3 shows the strength and direction of influence of each descriptor in the constructed model, assessed by determining the standard regression coefficient (X_j) and mean effect (AE) [24]. The molecular properties highlighted in Table 4 have correlation coefficients of 0.6. Table 5 presents the validity results of the internal assessment to ensure that the model is reliable. The results confirmed the stability and robustness of the model as valid because the calculated parameters were all in full agreement with the general validation criteria (Table 5).

Table 6 shows Y-Randomization parameters while Table 7 presents the threshold and coefficient of

Table 7 Random models parameters

Random models parameters	Mathematical expression	Threshold	Model
Average of the correlation coefficient for randomized data \bar{R}_r		$\bar{R} < 0.5$	0.4864
Average of determination coefficient for randomized data		$\bar{R}_r^2 < 0.5$	0.2538
Average of leave one out cross-validated determination coefficient for randomization data Q^2_r :		$\bar{Q}_r^2 < 0.5$	-0.39652
Coefficient for Y-randomization: cR_p^2	$R^2 \times \left(1 - \sqrt{ R^2 - \bar{R}_r^2 }\right)$	$cR_p^2 > 0.6$	0.6773

Table 8 External validation

Validation bounds	Mathematical expression	Threshold	Model	Comment
Slope of the plot of observed Activity versus calculated activity (k)	$\frac{\Delta Y_{cal}}{\Delta Y_{obs}}$	$0.85 < k < 1.15$	1.016	Passed
Slope of the plot of calculated versus observed activity values (k')	$\frac{\Delta Y_{obs}}{\Delta Y_{cal}}$	$0.85 < k < 1.15$	0.9210	Passed
$ r_0^2 - r_0'^2 $		< 0.3	0.0142	Passed
$\frac{r^2 - r_0'^2}{r^2}$		< 0.1	0.0032	Passed
$\frac{r^2 - r_0'^2}{r^2}$		< 0.1	0.00421	Passed
R_{test}^2	$1 - \frac{\sum (Y_{ext} - \bar{Y}_{ext})^2}{\sum (Y_{ext} - \bar{Y})^2}$	$R_{pred}^2 > 0.6$	0.7883	Passed

Y-randomization and Table 8 shows validation results for external assessment.

Figures 2 and 3 show graph of calculated activity versus observed activity of training set and graph of calculated activity versus observed activity of test set, respectively.

The William's graph shows the domain of applicability space (AD) shown in Fig. 4. The leverage value of compounds 10 and 15 was observed to be higher than the $h^* = 0.75$ (i.e. warning leverage).

3.5 Molecular docking studies

The results of the binding energy of the selected benzimidazolinone derivatives (compounds 13 and 21) and the reference drug to vital target proteins (AChE), implicated in the pathogenesis of AD from the molecular docking study are, respectively, shown in Figs. 5, 6, and 7.

Table 9 Pharmacokinetics of compounds 13 and 21

		Compound 13	Compound 21
Absorption	Caco2 permeability	0.823	1.035
	Intestinal absorption (human)	91.939	86.102
	Skin Permeability	-2.738	-2.735
Distribution	Volume of distributions	1.411	0.932
	Fraction unbound (human)	0.183	0.082
	BBB permeability	-0.024	-0.001
	CNS permeability	-2.192	-2.168
Metabolism	CYP2D6 substrate	Yes	Yes
	CYP3A4 substrate	Yes	Yes
Excretion	Total Clearance	0.623	0.906
	Renal OCT2 substrate	Yes	Yes
Toxicity	AMES toxicity	Yes	Yes
	Oral rat acute toxicity (LD50)	2.919	2.723
	Minnow toxicity	-0.674	0.257

3.6 Drug change assessment of selected compounds

We performed in silico ADMET studies on the two molecules reported in Tables 9 and 10 to supplement the results of 3D-QSAR and docking studies. Table 11 displays the physicochemical properties of compounds 13 and 21.

The predicted bioactivity scores of the selected compounds obtained Molinspiration software v2018.03 Chemoinformatics tools are given in Table 12.

Figure 8 exhibits the oral bioavailability graph of the two compounds on base of the six features discussed in physicochemical properties while Fig. 9 shows points located in the BOILED-Egg's, yolk of molecules 13 and 21.

4 Discussion

4.1 QSAR analysis

The considered model was carefully chosen and reported because it is statistically fit with the following assessment parameters as compared to other constructed model: R^2 of 0.937, R_{adj}^2 of 0.863, Q_{cv}^2 of 0.788, R_{test}^2 of 0.756, LOF of 0.0268, and cR_p^2 of 0.677. The selected model was found to have passed the minimum recommended values for validation of good QSAR models as reported in [24]. The details of the descriptors used in the model are listed in Table 2.

4.2 Mechanistic information of descriptors in the model built

Table 2 provides a comprehensive description of the molecular descriptors of the constructed models. Furthermore, the model showed a positive contribution from the descriptors AATS7i, MATS5p, and SpMin7_Bhe, but a negative contribution from the descriptor GATS6c. This means that an increase in the magnitude of AATS7i, MATS5p, and SpMin7_Bhe descriptors will positively influence the prediction of PIC_{50} with the

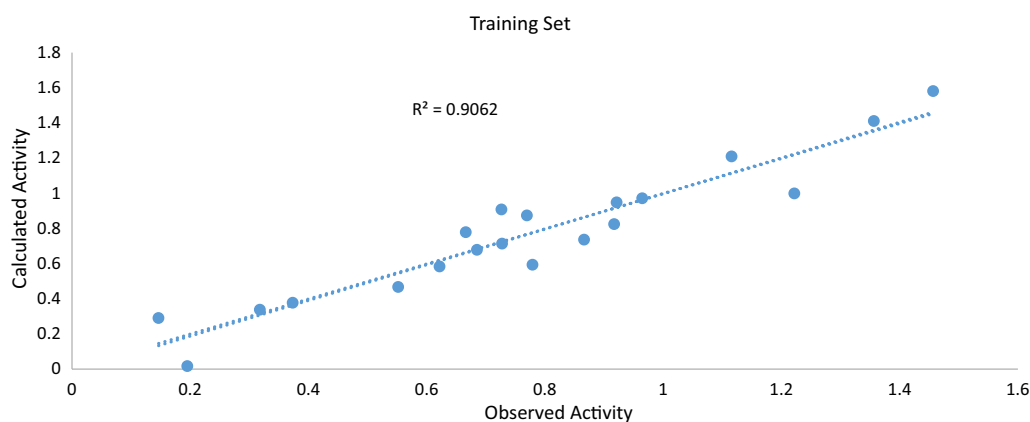


Fig. 2 Graph of calculated activity versus observed activity of training set

negative influence of the GATS6c descriptor. However, the AATS7i descriptor has the highest contribution, and is the most significant descriptor to be considered in the design of new hypothetical compounds. In addition, the signs of the regression coefficients for each descriptor indicated the direction of influence of the descriptors in the models, such that a positive regression coefficient associated with a descriptor will augment the activity profile of a compound, while the negative coefficient will diminish the activity of the compound.

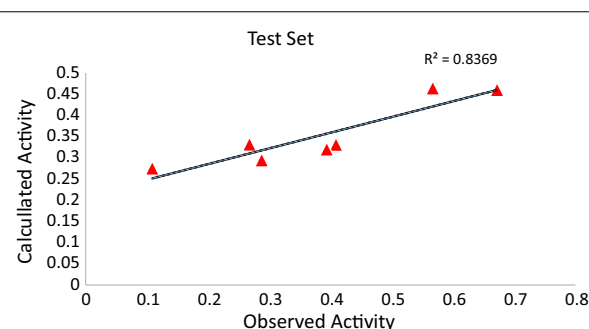


Fig. 3 Graph of calculated activity versus observed activity of test set

4.3 Derivation of the model and models and validation

The influence of each descriptor in the constructed model was assessed by determining standard regression coefficients X_j and AE [24]. Table 3 shows the strength and direction, as well as size and symbols for the X_j and AE values with which each descriptor influences the activity model. The connection between the descriptors and the activity of each compound was determined using ANOVA. The probability value for each descriptor at the 95% confidence level was found to be $p < \frac{1}{20} 1$, as shown in Table 3. Several statistical investigations were conducted on the calculated molecular properties in order to assess their validity.

The VIF was evaluated to define the extent of correlation between each descriptor. Generally, a VIF equal to $1 \geq 5$ signifies the non-existence of inter-correlations present in each of descriptor. However, $VIF \geq 10$ implies that the developed model is unsteady [25]. The VIF for each descriptor in the built model, which was found to be less than 5, as reported in Table 3, affirms that the descriptors were meaningfully orthogonal to each order because there was no inter-correlation between them. Therefore, the alternative hypothesis is accepted. This implies a direct connection between the biological activity of each

compound and the descriptors that influence the built model.

The molecular properties are highlighted in Table 4 with correlation coefficients of $< \pm 0.6$ correlation coefficient between them, which indicates that all properties were annulled of multicollinearity.

Table 5 shows the validity results of the internal assessment to guarantee that the model is reliable. The results confirmed the stability and robustness of the model as valid because the calculated parameters were all in full agreement with general validation criteria (Table 5).

Figures 2 and 3 show the graphs of calculated activity versus observed activity of a training set and a graph of calculated activity versus observed activity of a test set, respectively. It can be observed that the values of the test sets are in close agreement with the training set values.

William's graph shows the LAD, as shown in Fig. 4. The leverage values of compounds 10 and 15 were observed to be higher than $h^* = 0.75$ (is, warning leverage). Thus, it can be inferred that compounds 10 and 15 are influential molecules. Moreover, it was also observed that all the compounds were within the defined space of 2.5, which indicates that no compound is said to be an outlier.

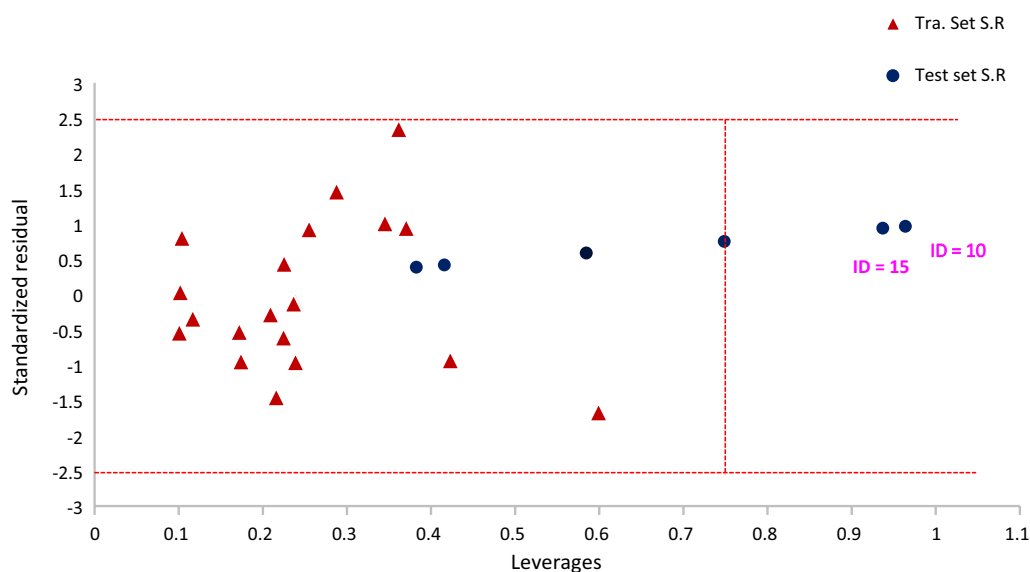


Fig. 4 Standardized residual activity versus observed activity

4.4 Molecular docking studies

The results of the binding energy of the selected benzimidazolinone derivatives (compounds 13 and 21) and the reference drug to a vital AChE implicated in the pathogenesis of AD from the molecular docking study are, respectively, shown in Figs. 5, 6, and 7, with the values for compounds 13 and 21 having a higher binding affinity for AChE than the approved drug. In order to study the binding mode and selectivity of most active compounds 34 and 38 with AChE (PDB code: 4MOE), Compound 13 was docked into the active site of the AChE domain protein with a splendid binding score of -11.2 kcal/mol involving the following interactions: conventional hydrogen bonding with Val281, Phe75, Met164, and carbon hydrogen bond-bonding, Asp76, Pro56, and Leu547Ala320, Ile77, and π -Alkyl interactions Trp168, Cys583, Pro594, His548 interactions are shown with their 3D interactions and surface interactions in Fig. 5. Compound 21 was docked into the active site of the AChE domain protein with an excellent binding score of 10.9 kcal/mol involving the following interactions: conventional hydrogen bonding with Asp211, Pro248, Lys411, and carbon hydrogen bonds Arg245, Pro431, Asp430, and π - σ bonding Arg245 and π -Alkyl interactions Arg245, Pro427, interactions shown with its 3D interactions and surface interactions are shown in Fig. 6. The reference compound docked into the active site of the AChE domain protein with an excellent binding score of 9.4 kcal/mol, involving the following interactions: Van der Waals bond Ser216, Carbon Hydrogen bond Thr208, Arg245, Glm207, Pi Cation interaction Lys411,—interaction Thr244, Amide-bonding Glu215

Table 10 Drug-likeness and medicinal chemistry of compounds 13 and 21

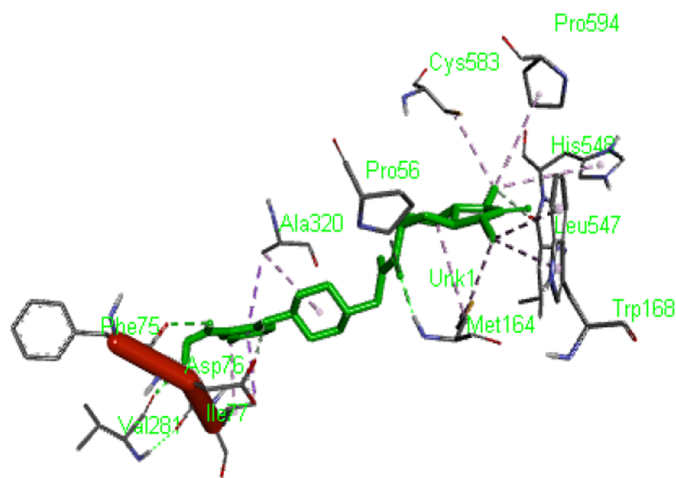
	Compound 13	Compound 21
Lipinski violations	0	0
Ghose violations	0	0
Veber violations	0	0
Egan violations	0	0
Muegge violations	0	0
Lead-likeness violations	1	2
PAINS alerts	0	0
Synthetic accessibility	3.30	2.85

and π -Alkyl interactions are shown with their 3D interactions and surface interactions in Fig. 7.

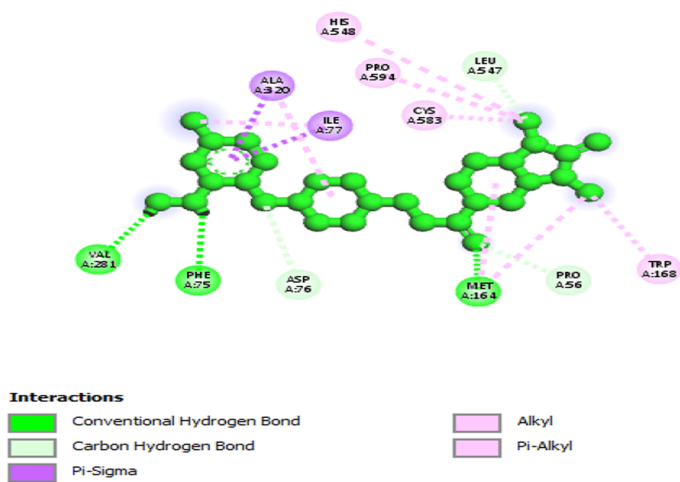
4.5 Drug change assessment of selected compounds

To supplement the findings of the 3D-QSAR and docking studies, we conducted in silico ADMET analyses of the two molecules listed in Tables 9 and 10. The ability to reach targets in bioactive form was assessed using the <http://swissadme.ch> and <http://biosig.unimelb.edu.au/pkcsn/web> platforms. The technologies of these webs employ a reasonable degree of certainty, as false-positive results are common in biochemical assays for small molecules [26].

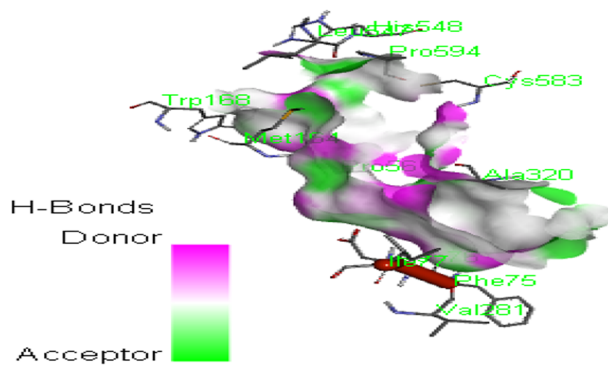
Table 9 indicates that the absorption characteristics of compounds 13 and 21 are capable of oral availability



A. Docking score of -11.2 kcal/mol

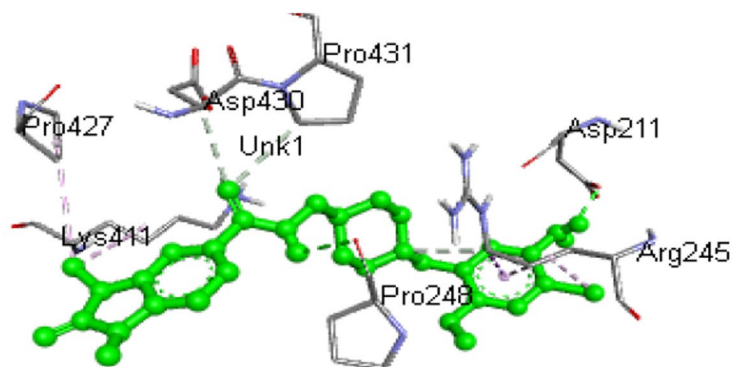


B.

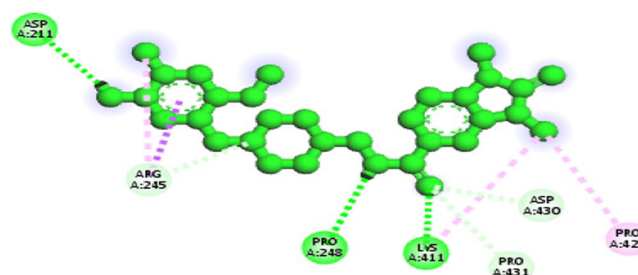


C. Stereoviews looking down the gorge of AChE binding with compound 13

Fig. 5 A and B show the 3D and 2D docking interactions between ligand 13 and receptor, respectively



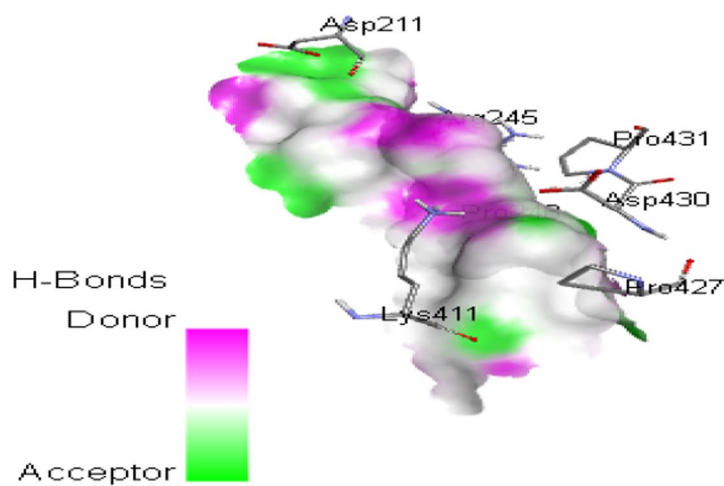
A. Docking score: -10.9 kcal/mol



Interactions

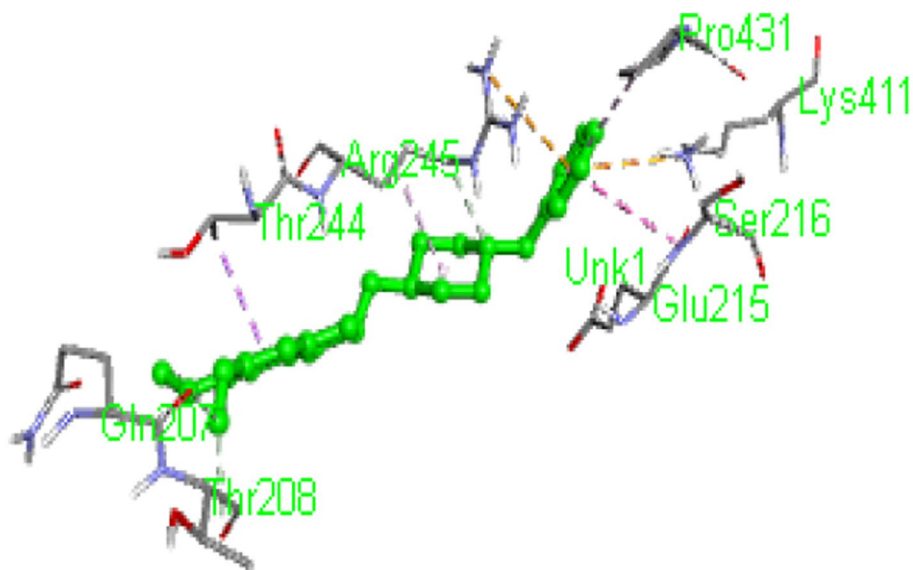
 Conventional Hydrogen Bond	 Alkyl
 Carbon Hydrogen Bond	 Pi-Alkyl
 Pi-Sigma	

(B).

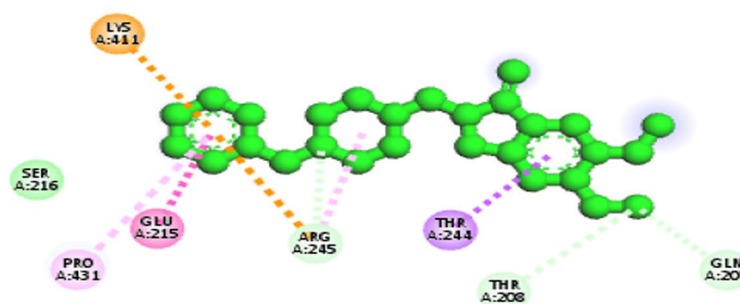


(C). Stereoviews looking down the gorge of AChE binding with compound

Fig. 6 A and B showed the 3D and 2D docking interactions between ligand 21 and receptor, respectively



(A). Docking score: -9.4 kcal/mol



Interactions

- | | |
|----------------------|------------------|
| van der Waals | Amide-Pi Stacked |
| Carbon Hydrogen Bond | Alkyl |
| Pi-Cation | Pi-Alkyl |
| Pi-Sigma | |

(B).

Fig. 7 Show the 3D and 2D interactions between donepezil and acetylcholinesterase

owing to optimal cell permeability. Human intestinal absorption and skin permeability were >0.8, >80% and < -2.5, respectively, are shown in Table 9.

The volume of distribution of the studied compounds was >0.45 which indicates that the drug is distributed in the plasma and describes the extent of drug distribution. Together with the unbound fraction, which labels the portion of free drug in plasma that may extravasate,

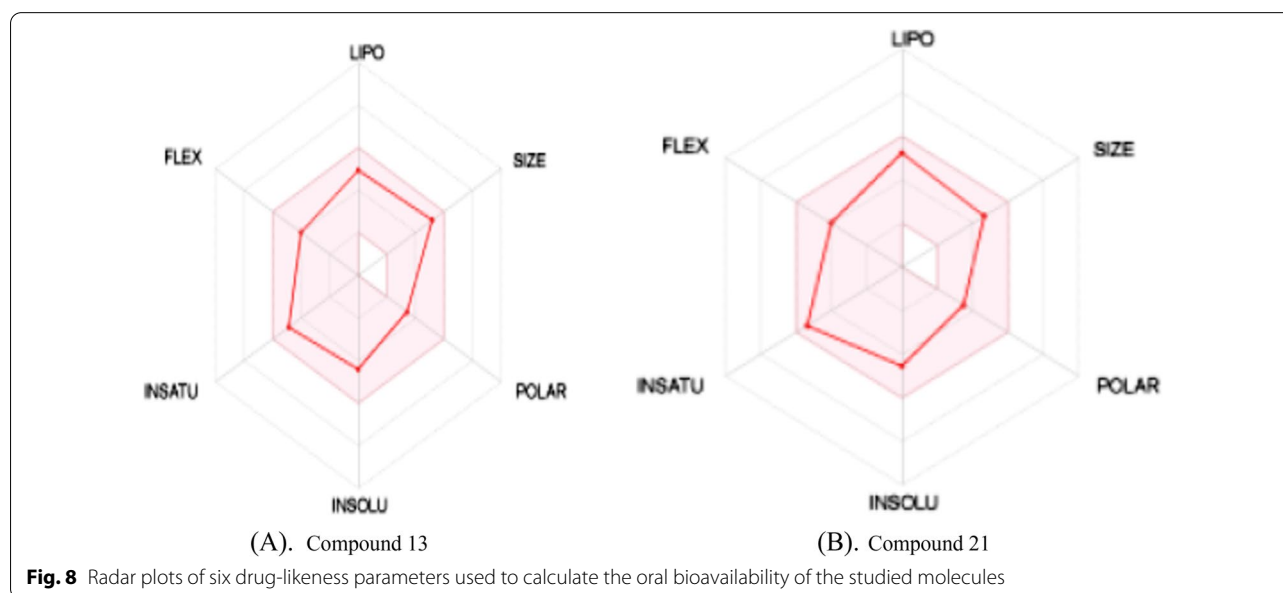
these are two of the most significant pharmacokinetic medication parameters. These two parameters have an adequate plasma distribution profile, with a fraction of the unbound drug between $0 \geq 0.157$. These values show that the molecules can circulate well and present an important unbound fraction in the plasma, thus becoming available to interact with the pharmacological target. The two compounds can penetrate the central nervous

Table 11 Physicochemical properties of compounds 13 and 21

Compounds	MW	HBA	HBD	MlogP	Lipinski violations	NRB	TPSA	WLogP
13	426.94	3	1	3.35	0	6	59.27	2.64
21	382.89	3	2	3	0	6	61.02	3.33

Table 12 Bioactivity score of the compounds

Compounds	GPCR ligand	Ion channel modulator	Kinase inhibitor	Nuclear receptor ligand	Protease inhibitor	Enzyme inhibitor
13	0.17	-0.02	0.06	-0.39	0.09	-0.06
21	0.32	0.21	0.26	-0.44	0.16	0.10



system owing to the volume of distribution and fraction unbound as indicated in Table 9.

As shown in Table 9, cytochrome P450 (CYP) molecules are indispensable information sources, this superfamily of isoenzymes is key players [27]. The synergy between CYP and P-gp can process small molecules to improve the protection of tissues and organisms [28]. Estimation of therapeutic molecules that are major isoform substrates (CYP2D6, CYP3A4, and CYP1A2) [29, 30]. Therefore, compounds 13 and 21 were brilliant CYP substrates.

Finally, from Table 9, the expected values of the total clearance, which measures the efficiency of the body in eliminating a drug, indicate that the two compounds have a noble renal elimination and are not substrates of the renal organic cation transporter 2 (OCT2). In conclusion,

the compounds passed the AMES and Minnow toxicity tests, and did not present any particular toxicity problems. The overall analysis of Table 9 highlights that compounds 13 and 21 could be outstanding candidates as drugs, or could lead to further studies and manipulations.

Table 10 displays other drug-likeness rules, such as Ghose, Veber, Egan, and Muegge violations, and all are satisfied by the two molecules that will provide the lead like rule with high affinity in high-throughput screens that allow for the discovery and exploitation of additional interactions in the lead-optimization phase [31–34]. Furthermore, the PAINS model, which was designed to exclude small molecules that are likely to produce false positives in biological assays, paid no attention to compounds 13 and 21.

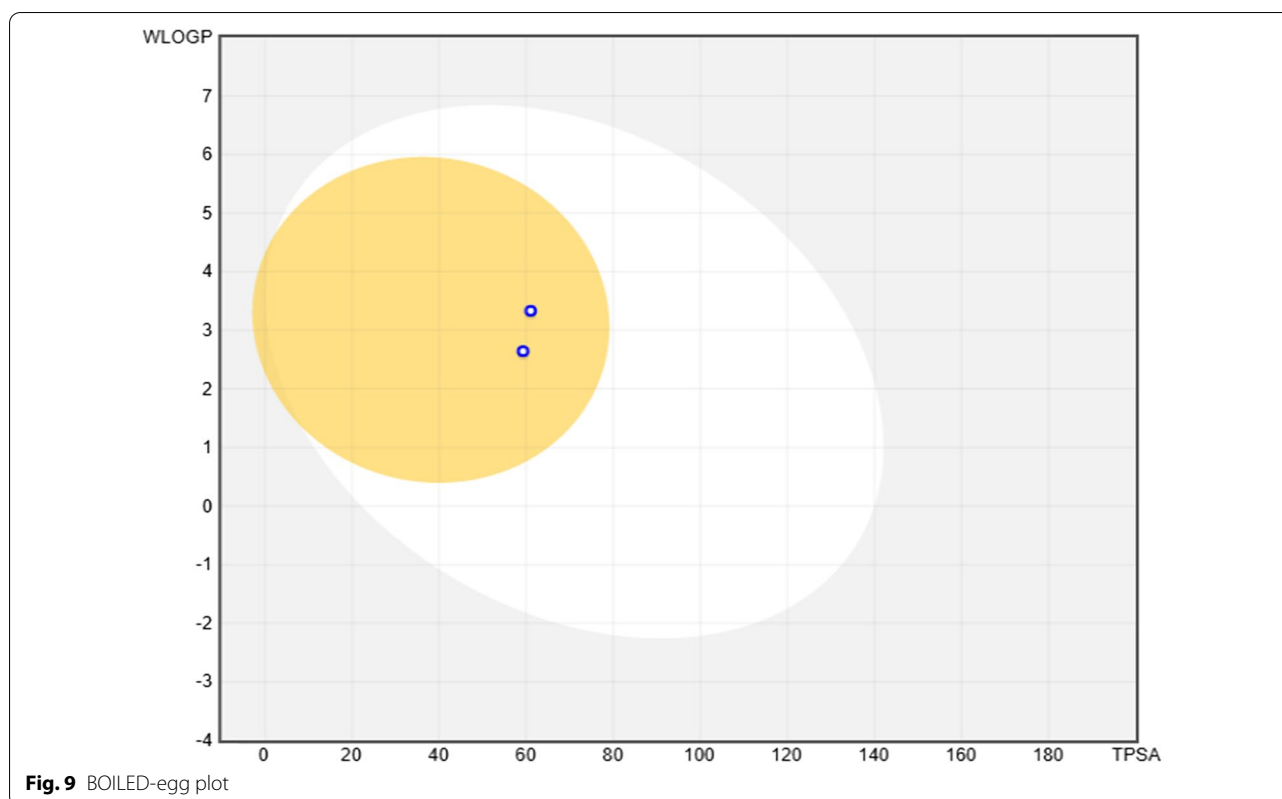


Fig. 9 BOILED-egg plot

Table 11 lists the physicochemical properties of compounds 13 and 21. The compounds passed Lipinski's rule of five [35]. This further demonstrates the druggability of these compounds.

The predicted bioactivity scores of the selected compounds obtained using the Molinspiration software v2018.03 Chemoinformatics tools are given in Table 12. For the bioactivity score, the G protein coupled receptor (GPCR) ligand was active for both compounds, with value of 0.32 and 0.17. In [36], modulators of ion channels permit charged particles across cell membranes, and they are an important receptor in the healing tract. These two compounds were found to be active. All the compounds were moderately active as kinase inhibitors. In a previous study [37], Nuclear receptors play a combinatorial role in inflammation and immunity. The two compounds were active, but compound 13 was more active in terms of protease inhibitor bioactivity scores. The two compounds were moderately active. The values for enzyme inhibition showed that all compounds were highly active. The activity score profile of the compounds showed that they were biologically active and have physiological influence.

Figure 8 illustrates the oral bioavailability graph of the two compounds on the basis of the six features discussed in physicochemical properties. The compounds have shown results within these limits, and these two

compounds have good physico-chemical profile, a necessary parameter in drugs or clinical trials. The six physicochemical properties are lipophilicity, size, polarity, solubility, flexibility, and saturation. Descriptors were used on each axis to define physicochemical range [38, 39]. The pink region was the drug-like consideration of the molecule in the radar graph. The compounds obey Lipinski's rule of five. Therefore, the two compounds displayed values within the interval known for medicine.

Figure 9 shows points located in the BOILED-Egg's yolk that signified the molecules predicted to passively permeate through the blood–brain barrier, whereas the egg white was relative to the molecules predicted to be passively absorbed by the gastrointestinal tract. Blue dots indicate the molecules which emanate from the central nervous system with the aid of P-glycoprotein. Overall, the plot showed that compounds 13 and 21 have excellent bioavailability.

5 Conclusions

A well-validated and robust QSAR model was constructed for compounds 13 and 21 with anti-Alzheimer activity against the AChE protein receptor. The computational studies, QSAR, docking, and ADMET studies proved that these compounds have high binding affinity towards the targeted AChE protein receptor and revealed

the binding energies of these compounds, which showed that there is plausibility of inhibiting the AChE protein. Overall, the present study acts as evidence to prove that these compounds from 1,3-dimethylbenzimidazolinone derivatives have the capacity to inhibit the AChE protein receptor, which also paves the way for the two compounds to be screened for AChE protein. In other words, this study with the QSAR, docking, and drug-like properties in primarily pharmacokinetic studies will be positioned as a foundation for carrying out *in vitro* and *in vivo* studies in the future.

Abbreviations

AD: Alzheimer's disease; ADMET: Absorption, distribution, metabolism, excretion, and toxicity; AChE: Acetylcholinesterase; AE: Mean effect; BOILED-egg: Brain or intestinal estimated permeation method; BBB: Blood–brain barrier; CADD: Computer-aided drug design; DFT: Density functional theory; GFA: Genetic function approximation; HIA: Human gastrointestinal absorption; HBA: Hydrogen bond acceptor; HBD: Hydrogen bond donor; LOF: Lack of fit; LAD: Leverage applicability domain; MLR: Multi-linear regression; MW: Molecular weight; NRB: Number of rotatable bonds; PAINS: PAINS Pan assay interference compounds; QSAR: Quantitative structural activity relationship; SE: Standard error; TPSA: Topological polar surface area; VIF: Variance inflation factor; Xi: Regression coefficient.

Acknowledgements

The authors gratefully acknowledged the technical effort of Dr. Abdulfatai Usman, Mr. Stephen Ejeh, and Mr. Samuel Adawara all of Chemistry Department, Ahmadu Bello University, Zaria.

Author contributions

AA designed and wrote the manuscript; UA, GAS, and AES supervised and carried out the statistical analysis. All authors read and approved the final manuscript.

Funding

Not applicable.

Availability of data and materials

Not applicable.

Declarations

Ethics approval and consent to participate

Not applicable.

Consent for publication

Not applicable.

Competing interests

The authors declare that they have no competing interests.

Received: 26 July 2021 Accepted: 29 March 2022

Published online: 11 April 2022

References

- Salthouse TA (2004) What and when of cognitive aging. *Curr Dir Psychol Sci* 13(4):140–144. <https://doi.org/10.1111/j.0963-7214.2004.00293.x>
- Qiang W, Yau W, Lu J, Collinge J, Tycko R (2017) Letter. *Nature*. <https://doi.org/10.1038/nature20814>
- Huang W, Zhang X, Chen W (2016) 2016 Role of oxidative stress in Alzheimer's disease (review). *Nature*. <https://doi.org/10.3892/br.2016.630>
- Bru C, Leonetti F, Altomare C, Carotti A (2001) Brief articles. *Nature* 66:3195–3198
- Thirathmatrakul S, Yenjai C, Waiwut P, Vajragupta O (2014) European Journal of Medicinal Chemistry Synthesis, biological evaluation and molecular modeling study of novel tacrine e carbazole hybrids as potential multifunctional agents for the treatment of Alzheimer's disease. *Eur J Med Chem* 75:21–30. <https://doi.org/10.1016/j.ejmech.2014.01.020>
- Samadi A, Valderas C, Ríos CDL et al (2011) Cholinergic and neuroprotective drugs for the treatment of Alzheimer and neuronal vascular diseases. II. Synthesis, biological assessment, and molecular modelling of new tacrine analogues from highly substituted 2-aminopyridine-3-carbonitriles. *Bioorgan Med Chem* 19(1):122–133. <https://doi.org/10.1016/j.bmc.2010.11.040>
- Association A (2015) 2015 Alzheimer's disease facts and figures. *Alzheimer's Dementia* 11(3):332–384. <https://doi.org/10.1016/j.jalz.2015.02.003>
- Ihalainen J, Sarajärvi T, Rasmussen D et al (2011) Neuropharmacology Effects of memantine and donepezil on cortical and hippocampal acetylcholine levels and object recognition memory in rats. *Neuropharmacology* 61(5–6):891–899. <https://doi.org/10.1016/j.neuropharm.2011.06.008>
- Wu X, Zeng H, Zhu X, Ma Q, Hou Y, Wu X (2013) European Journal of Pharmaceutical Sciences Novel pyrrolopyridinone derivatives as anticancer inhibitors towards Cdc7: QSAR studies based on dockings by solvation score approach. *Eur J Pharm Sci* 50(3–4):323–334. <https://doi.org/10.1016/j.ejps.2013.07.013>
- Li P, Jia J, Fang M, Zhang L, Guo M, Xie J (2014) *In vitro and in vivo* ACE inhibitory of pistachio hydrolysates and *in-silico* mechanism of identified peptide binding with ACE. *Process Biochem* 49(5):898–904. <https://doi.org/10.1016/j.procbio.2014.02.007>
- Mo J, Chen T, Yang H et al (2020) dimethylbenzimidazolinones as cholinesterase inhibitors against Alzheimer's disease. *Nature*. <https://doi.org/10.1080/14756366.2019.1699553>
- Adeniji SE, Uba S, Uzairu A (2018) QSAR modeling and molecular docking analysis of some active compounds against mycobacterium tuberculosis receptor (Mtb CYP121). *J Pathogens* 2018:1–24. <https://doi.org/10.1155/2018/1018694>
- Oluwaseye A, Uzairu A, Shallangwa GA, Abechi SE. *Journal of King Saud University—Science Quantum chemical descriptors in the QSAR studies of compounds active in maxima electroshock seizure test*; 2018.
- Adeniji SE, Uba S, Uzairu A (2018) *Journal of King Saud University – Science Theoretical modeling for predicting the activities of some active compounds as potent inhibitors against Mycobacterium tuberculosis using GFA-MLR approach*. *J King Saud Univ Sci*. <https://doi.org/10.1016/j.jksus.2018.08.010>
- Adeniji SE, Uba S, Uzairu A (2020) Quantitative structure–activity relationship and molecular docking of 4-Alkoxy-Cinnamic analogues as anti-mycobacterium tuberculosis. *J King Saud Univ Sci* 32(1):67–74. <https://doi.org/10.1016/j.jksus.2018.02.005>
- Abdulfatai U, Uzairu A, Uba S, Shallangwa GA (2019) Molecular modelling and design of lubricant additives and their molecular dynamic simulations studies of Diamond-Like-Carbon (DLC) and steel surface coating. *Egypt J Pet* 28(1):111–115. <https://doi.org/10.1016/j.ejpe.2018.12.004>
- Tropsha A, Golbraikh A. *Predictive QSAR Modeling Workflow, Model Applicability Domains, and Virtual Screening*. *Nature* 2007 66:3494–3504.
- Ajala A, Uzairu A, Suleiman IO, Uttu AJ (2018) Theoretical investigation of correlations between molecular and electronic structure and antifungal activity in coumarin derivatives: combining Qsar and Dft studies. *J Adv Med Pharma* 16(3):1–18. <https://doi.org/10.9734/JAMPS/2018/22801>
- Roy K, Mitra J, Kar S, Ojha PK, Das RN, Kabir H. Comparative studies on some metrics for external validation of QSPR models. 2012.
- Veerasamy R, Rajak H, Jain A, Sivadasan S. Validation of QSAR models—strategies and importance validation of QSAR models—strategies and importance. 2011. April 2019.
- Paul Gleeson M, Hersey A, Hannongbua S (2011) *In-silico ADME models: a general assessment of their utility in drug discovery applications*. *Curr Top Med Chem* 11(4):358–381. <https://doi.org/10.2174/156802611794480927>
- Daina A, Michielin O, Zoete V (2017) SwissADME: a free web tool to evaluate pharmacokinetics, drug-likeness and medicinal chemistry friendliness of small molecules. *Sci Rep* 7:1–13. <https://doi.org/10.1038/srep42717>
- Ambure P, Aher RB, Gajewicz A, Puzyn T, Roy K (2015) "NanoBRIDGES" software: open access tools to perform QSAR and nano-QSAR modeling.

- Chemom Intell Lab Syst 147:1–13. <https://doi.org/10.1016/j.chemolab.2015.07.007>
24. Tropsha A (2010) Best practices for QSAR model development, validation, and exploitation. *Mol Inf* 29(6–7):476–488. <https://doi.org/10.1002/minf.201000061>
 25. Beheshti A, Pourbasheer E, Nekoei M (2012) QSAR modeling of antimalarial activity of urea derivatives using genetic algorithm—multiple linear regressions. *J Saudi Chem Soc* 1:1–9. <https://doi.org/10.1016/j.jscs.2012.07.019>
 26. Matlock MK, Hughes TB, Dahlin JL, Swamidass SJ (2018) Modeling small-molecule reactivity identifies promiscuous bioactive compounds. *J Chem Inf Model* 58(8):1483–1500. <https://doi.org/10.1021/acs.jcim.8b00104>
 27. Enzymes T (2007) The biochemistry of drug metabolism—an introduction. *Chem Biodivers* 4:2031–2122
 28. Van Waterschoot RAB, Schinkel AH (2011) A critical analysis of the interplay between cytochrome P450 3A and P-Glycoprotein: recent insights from knockout and transgenic mice. *Pharmacol Rev* 63(2):390–410. <https://doi.org/10.1124/pr.110.002584>
 29. Di L, Di L (2014) The role of drug metabolizing enzymes in clearance. *Expert Opin Drug Metab Toxicol*. <https://doi.org/10.1517/17425255.2014.876006>
 30. Wolf CR, Smith G, Smith RL (2000) Clinical review. *Br Med J* 320:987–990
 31. Egan WJ, Merz KM, Baldwin JJ (2000) Prediction of drug absorption using multivariate statistics. *J Med Chem* 43(21):3867–3877. <https://doi.org/10.1021/jm000292e>
 32. Ghose AK, Viswanadhan VN, Wendoloski JJ (1999) A knowledge-based approach in designing combinatorial or medicinal chemistry libraries for drug discovery. 1. A qualitative and quantitative characterization of known drug databases. *J Combin Chem* 1(1):55–68. <https://doi.org/10.1021/cc9800071>
 33. Muegge I, Heald SL, Brittelli D (2001) Simple selection criteria for drug-like chemical matter. *J Med Chem* 44(12):1841–1846. <https://doi.org/10.1021/jm015507e>
 34. Veber DF, Johnson SR, Cheng HY, Smith BR, Ward KW, Kopple KD (2002) Molecular properties that influence the oral bioavailability of drug candidates. *J Med Chem* 45(12):2615–2623. <https://doi.org/10.1021/jm020017n>
 35. Lipinski CA (2016) Rule of five in 2015 and beyond: target and ligand structural limitations, ligand chemistry structure and drug discovery project decisions. *Adv Drug Deliv Rev* 101:34–41. <https://doi.org/10.1016/j.addr.2016.04.029>
 36. Linn C, Roy S, Samant LR, Chowdhary A (2015) Research article in-silico pharmacokinetics analysis and ADMET of phytochemicals of Datura. *J Chem Pharm Res* 7(11):385–388
 37. Glass CK, Ogawa S (2006) Combinatorial roles of nuclear receptors in inflammation and immunity. *Nat Rev Immunol* 6:44–55. <https://doi.org/10.1038/nri1748>
 38. Ritchie TJ, Ertl P, Lewis R (2011) The graphical representation of ADME-related molecule properties for medicinal chemists. *Drug Discov Today* 16(1–2):65–72. <https://doi.org/10.1016/j.drudis.2010.11.002>
 39. Lovering F, Bikker J, Humblet C (2009) Escape from Flatland: increasing saturation as an approach to improving clinical success. *J Med Chem*. <https://doi.org/10.1021/jm901241e>

Publisher's Note

Springer Nature remains neutral with regard to jurisdictional claims in published maps and institutional affiliations.

Submit your manuscript to a SpringerOpen[®] journal and benefit from:

- Convenient online submission
- Rigorous peer review
- Open access: articles freely available online
- High visibility within the field
- Retaining the copyright to your article

Submit your next manuscript at ► [springeropen.com](https://www.springeropen.com)
